Convergent evolution of SARS-CoV-2 XBB lineages on receptor-binding domain 455-456 enhances antibody evasion and ACE2 binding

Fanchong Jian[1,2,3,#], Sijie Yang[1,4,#], Yuanling Yu[2,#], Weiliang Song[1,2,5], Ayijiang Yisimayi[1,2,5], Xiaosu Chen[6], Yanli Xu[7], Peng Wang[2], Lingling Yu[2], Jing Wang[2], Lu Liu[2], Xiao Niu[1,5], Jing Wang[1,2,5], Tianhe Xiao[1,8], Ran An[2], Yao Wang[2], Qingqing Gu[2], Fei Shao[2], Ronghua Jin[7], Zhongyang Shen[9], Youchun Wang[2,10], Yunlong Cao[1,2,5,*]

[1]Biomedical Pioneering Innovation Center (BIOPIC), Peking University, Beijing, P. R. China.

[2]Changping Laboratory, Beijing, P. R. China.

[3]College of Chemistry and Molecular Engineering, Peking University, Beijing, P. R. China.

[4]Peking-Tsinghua Center for Life Sciences, Tsinghua University, Beijing, P. R. China.

[5]School of Life Sciences, Peking University, Beijing, P. R. China.

[6]Institute for Immunology, College of Life Sciences, Nankai University, Tianjin, P. R. China.

[7]Beijing Ditan Hospital, Capital Medical University, Beijing, P. R. China.

[8]Joint Graduate Program of Peking-Tsinghua-NIBS, Academy for Advanced Interdisciplinary Studies, Peking University, Beijing, P. R. China.

[9]Organ Transplant Center, NHC Key Laboratory for Critical Care Medicine, Tianjin First Central Hospital, Nankai University, Tianjin, P. R. China.

[10]Institute of Medical Biotechnology, Chinese Academy of Medical Science & Peking Union Medical College, Kunming, P. R. China

[*]Correspondence: Yunlong Cao (yunlongcao@pku.edu.cn).

[#]These authors contributed equally.

Summary

Severe acute respiratory syndrome coronavirus 2 (SARS-CoV-2) XBB lineages have achieved dominance worldwide and keep on evolving. Convergent evolution of XBB lineages on the receptor-binding domain (RBD) L455F and F456L is observed, resulting in variants like EG.5, FL.1.5.1, XBB.1.5.70, and HK.3. Here, we show that neutralizing antibody (NAb) evasion drives the convergent evolution of F456L, while the epistatic shift caused by F456L enables the subsequent convergence of L455F through ACE2 binding enhancement and further immune evasion. Specifically, L455F and F456L evades Class 1 NAbs, which could reduce the neutralization efficacy of XBB breakthrough infection (BTI) and reinfection convalescent plasma. Importantly, L455F single substitution significantly dampens receptor binding; however, the combination of L455F and F456L forms an adjacent residue flipping, which leads to enhanced NAbs resistance and ACE2 binding affinity. Our results indicate the evolution flexibility contributed by epistasis cannot be underestimated, and the evolution potential of SARS-CoV-2 RBD remains high.

Highlights

- L455F and F456L enhance the resistance to Class 1 NAbs
- L455F and F456L lower neutralization of XBB BTI convalescent plasma
- L455F+F456L flipping significantly increases ACE2 binding affinity

Severe acute respiratory syndrome coronavirus 2 (SARS-CoV-2) has been continuously circulating and evolving worldwide [1-4]. Since late 2022, XBB* variants, especially XBB.1.5 and other XBB derivatives with a proline on residue 486 (486P) on the receptor-binding domain (RBD) of the virus Spike glycoprotein (S) started to dominate, which demonstrated enhanced binding to human ACE2 while maintaining extremely strong capability of evading humoral immunity [5-8]. These immune-evasive lineages are still continuously accumulating more S mutations, such as R403K, V445S, L455F, F456L and K478R, that may lead to further shift in antigenicity and escape from neutralizing antibodies elicited by repeated vaccination and infection [9,10]. Some immune escape mutations, represented by F456L, even convergently appeared recently in multiple independent XBB derivative strains, such as EG.5, XBB.1.5.10, FE.1 and FD.1.1, indicating strong selection pressure due to herd immunity (Figure 1A) [11,12]. By August 2023, over 40% of newly uploaded SARS-CoV-2 sequences carry F456L mutation. Furthermore, multiple independent XBB lineages with both F456L and L455F are growing rapidly in different countries, such as XBB.1.5.70/GK.* in Brazil, the United States, and Canada, and HK.3 (EG.5.1.1.3) in China (Figure 1B-C) [12-14]. However, the lineages with L455F mutation but without F456L did not exhibit any growth advantage [13]. Interestingly, L455 and F456 are two adjacent residues on the receptor-binding motif (RBM) of SARS-CoV-2 RBD, and the variant is just the "flipping" of the two residues, L455-F456 to F455-L456 (Figure 1B). It is crucial to investigate the impacts on immune evasion and infection efficiency, and the underlying mechanism of such epistasis that enables the unexpected advantage of L455F mutation on the basis of XBB*+F456L lineages.

To interrogate whether L455F, F456L, and their combination leads to enhanced resistance to neutralizing antibodies elicited by vaccination and infection, we collected plasma samples from three cohorts with distinct SARS-CoV-2 immunization histories. All participants in the three cohorts had received triple doses of CoronaVac or BBIBP/WIBP/CCIBP-CorV (inactivated vaccines based on SARS-CoV-2 ancestral strain developed by Sinovac and Sinopharm, respectively) before any known infection [15,16]. The first cohort includes participants who were breakthrough-infected by BA.5 or BF.7 (66 samples), the second infected by XBB* with S486P (mainly XBB.1.9.1/XBB.1.9.2, 27 samples), and the third experienced BA.5/BF.7 BTI before XBB*+486P reinfection (mainly XBB.1.9.1/XBB.1.9.2, 54 samples). The infected strains were inferred from the epidemiological data and uploaded SARS-CoV-2 sequences in Beijing and Tianjin, China, where

the patients were recruited, during the infections (Table S1). We evaluated their neutralization activities against SARS-CoV-2 D614G (B.1), BA.5, XBB.1.5, XBB.1.16 (XBB.1+E180V+K478R+S486P), XBB.1.5+F456L (represented by EG.5), EG.5.1 (EG.5+Q52H), XBB.1.5+F456L+K478R (represented by FL.1.5.1), and XBB.1.5+L455F+F456L (represented by XBB.1.5.70) spike-pseudotyped vesicular stomatitis virus (VSV) (Figure 2A). Consistent with previous studies, single BA.5/BF.7 or XBB breakthrough infection (BTI) cannot elicit NAbs that efficiently neutralize all XBB subvariants due to immune imprinting, with 50% neutralization titers (NT50) lower than 100 [9,17]. In contrast, convalescent plasma samples from the reinfection cohort exhibit higher titers against BA.5 than D614G and neutralize XBB subvariants well, which indicates that second exposure to Omicron helps alleviate imprinting. Notably, compared to F456L which is known to escape many NAbs elicited by Omicron reinfection, the additional L455F substitution further causes substantial evasion of plasma from the reinfection cohort (Figure 2A) [18].

As residues 455 and 456 on RBD are mainly recognized by Class 1 antibodies, which is also referred to as "Group A1/A2" in our previous study, we tested the pseudovirus-neutralizing activities of a panel of XBB.1.5-effective RBD-targeting monoclonal NAbs against these newly-emerged XBB subvariants. The tested mAbs are expected to target 455/456 as determined by deep mutational scanning (DMS) (Figure 2B). L455F and F456L single substitution escape 11 and 8 out of 34 Group A1/A2 NAbs, respectively. Their combination exhibits stronger evasion, against which only 8 NAbs remain effective. Notably, 11 NAbs were not completely escaped by either L455F or F456L, but escaped by the combination, indicating the synergy of the two mutations (Figure 2C). We also evaluated the activity of neutralizing mAbs reported as drug candidates, including three that had been approved for emergency use. Two of three tested Class 1 NAbs, BD57-0129 and Omi-42, were partially evaded by L455F and L455F+F456L, while BD56-1854 remains potent [19]. The activity of Class 3 antibody S309 (Sotrovimab) is not substantially affected, remaining weak neutralization [20]. As expected, SD1-targeting antibody S3H3, and our previously reported Class 1/4 (Group F3) RBD-targeting therapeutic neutralizing antibody SA55 remain potent against all tested XBB subvariants, given that the mutated residues in the variants are not directly recognized by SA55 and S3H3 (Figure 2D) [21,22].

The above results demonstrate that both the L455F and F456L mutations can confer resistance to neutralization by convalescent plasma, primarily mediated by escaping Class 1 neutralizing

antibodies. However, it remains unclear why, during natural evolution, various lineages consistently evolve F456L independently, followed by subsequent occurrence of the L455F mutation, while cases where L455F is acquired first are rarely observed. Due to the fact that residues 455-456 are located on the RBM of RBD, we hypothesize that the effects of the L455F and F456L combination originate from their impact on the affinity for the receptor, human ACE2 (hACE2). Previous DMS data have indicated that individual substitutions, L455F or F456L, both lead to a substantial decrease in hACE2 affinity within the BA.2 background. However, as the combination of these two mutations essentially results in an adjacent residue flipping, there might be a local compensatory effect on hACE2 binding. The significant antigenic shift from BA.2 to XBB.1.5 may also alter the impacts of the two mutations on receptor binding. To validate the hypothesis, we constructed recombinant RBD subunits for XBB.1.5, XBB.1.5+L455F, XBB.1.5+F456L, and XBB.1.5+L455F+F456L, and determined their binding affinities (dissociation equilibrium constant) to hACE2 by surface plasmon resonance (SPR) assays, which demonstrate 6.4 nM, 25 nM, 11 nM, and 2.5 nM, respectively (Figure 2E and S1). Consistent with DMS results, L455F significantly dampens hACE2-binding affinity of XBB.1.5 RBD, and F456L also slightly weakens the binding to hACE2. Surprisingly, although neither of the two mutations increases hACE2 affinity alone, their combination XBB.1.5+L455F+F456L exhibits significantly higher affinity than XBB.1.5.

In this study, we evaluated the impacts of L455F and F456L, two frequently emerging adjacent mutations that convergently occur in multiple XBB sublineages, on antibody neutralization and receptor binding. We demonstrate that L455F further evades Class 1 NAbs on the XBB.1.5+F456L basis, while single F456L or L455F substitution dampens ACE2 binding. Surprisingly, their combination, which is exactly a “Lys-Phe” to “Phe-Lys” flipping between adjacent residues on the ACE2 binding interface, dramatically enhances affinity to ACE2. Together, these results explain the convergent evolution of XBB subvariants which evolve F456L and L455F in succession. Epistasis is a genetic phenomenon that the effect of one mutation is dependent on the presence of other mutations, resulting in non-additive impacts of mutations on specific functions [23,24]. A previous study reported the epistatic interaction between two early SARS-CoV-2 RBD mutations on RBD, Q498R and N501Y [25]. Based on the ancestral SARS-CoV-2 RBD, Q498R alone slightly reduced ACE2 binding affinity, while a strong enhancement in affinity is observed for Q498R based on N501Y (Alpha VOC). The epistatic shift described here is even more striking. L455F caused strong

affinity reduction on XBB.1.5, but significantly improved the hACE2-binding affinity of XBB.1.5+F456L. Both L455 and F456 are on the core of the RBD-hACE2 interface, forming a compact conformation with D30 and K31 on ACE2 (Figure S2A) [26]. The L455F mutation is likely to clash with F456 and leads to a local conformational change, which may dampen the interaction with ACE2. However, if F456 is mutated to the smaller leucine, the local conformation is likely to be kept (Figure S2B). ACE2 mimicry has been considered to be a useful strategy for identifying and designing broad-spectrum SARS-CoV-2-neutralizing binders and antibodies [27,28]. Class 1 public NAbs, such as Omi-42, interact with RBD L455/F456 with heavy chain CDR3 in a distinct way compared to ACE2 (Figure S2C) [19]. Similarly, most XBB.1.5-effective Class 1 NAbs failed to mimic the binding mode of ACE2 and escaped by XBB.1.5+L455F+F456L. The emergence of L455F+F456L indicates that such receptor mimicry could be extremely difficult. To achieve the goal that mutants escaping the neutralizer also lose affinity to the receptor, the binder should not only target the same residues as those targeted by the receptor, but also mimic the binding mode of the receptor. To further investigate and explain such phenomenon, detailed experimental structural analyses and computational simulation of XBB.1.5 RBD with these two mutations in complex with ACE2 should be necessary in the future.

Overall, our data rationalized the emergence and circulation of XBB sublineages with F456L followed by L455F mutation, and highlighted the enhanced receptor-binding affinity and neutralizing antibody escape, which may lead to higher transmissibility and risk of breakthrough infection and reinfection. Considering the continuously increasing proportion of these variants, the efficacy of developing NAb drugs and vaccines against them should be carefully evaluated. Epistasis could substantially extend the evolution flexibility of SARS-CoV-2 RBD, leading to novel mutants with extremely high capability of escaping NAbs without great compromise on infectivity. The evolutionary potential of SARS-CoV-2 RBD is still high, and should not be underestimated.

Acknowledgments

We are grateful to scientists in the community for their continuous tracking of SARS-CoV-2 variants and helpful discussion, including Jesse Bloom, Daniele Focosi, Ryan Hisner, Cornelius Roemer, Federico Gueli, Tom Peacock, Raj Rajnarayanan, and many other researchers. We thank all volunteers for providing the blood samples. This project is financially supported by the Ministry of

Science and Technology of China （2023YFC3041500；2023YFC3043200）, and Changping Laboratory (2021A0201; 2021D0102), and National Natural Science Foundation of China (32222030).

Author Contributions

Y.C. designed and supervised the study. F.J. and Y.C. wrote the manuscript with inputs from all authors. Q.G. proofread the manuscript. S.Y., W.S. and F.J. performed sequence analysis and illustration. Y.Y. and Youchun W. constructed pseudoviruses. J.W. (BIOPIC) and F.J. analyzed the DMS data. J.W. (Changping Laboratory), L.L, L.Y. and F.S. performed protein expression and purification experiments. P.W., L.Y., T.X., R.A., Yao W. and F.S. processed the plasma samples and performed the pseudovirus neutralization assays, ELISA, and SPR. W.S., A.Y., X.N. and Y.C. analyzed the neutralization data. Y.X., X.C., Z.S. and R.J. recruited the SARS-CoV-2 convalescents.

Declaration of interests

Y.C. is one of the inventors of the provisional patent applications for BD series antibodies, which includes SA55 (BD55-5514). Y.C. is one of the founders of Singlomics Biopharmaceuticals. Other authors declare no competing interests.

Figure Legends

Figure 1 | Convergent evolution and circulation of SARS-CoV-2 XBB variants

(A) RBD mutations carried by emerging XBB subvariants. L455F, F456L, and K478R are observed in multiple independent lineages, demonstrating high selection pressure and convergent evolution.

(B) Structural representation of the position of two convergently mutated residues L455 and F456 (colored in red) on the receptor-binding motif of XBB.1 RBD in complex with human ACE2 (colored in brown) (PDB: 8IOU).

(C) Proportion of XBB subvariants since March 2023 with S486P (represented by XBB.1.5), S486P+F456L (represented by EG.5), or S486P+L455F+F456L (represented by XBB.1.5.70) among uploaded sequences in the World, Brazil, China, and United States. F456L and L455F exhibit growth advantage compared to their ancestor (XBB*+S486P).

Figure 2 | Emerging XBB subvariants further evade neutralizing antibodies

(A) 50% neutralization titers against SARS-CoV-2 variants of convalescent plasma from individuals who received triple doses of CoronaVac and breakthrough-infected by BA.5/BF.7 (n=66), XBB*+486P (n=27), or BA.5/BF.7 followed by XBB*+486P reinfection (n=54). VSV-based pseudoviruses are used. Statistical significances and geometric mean titer (GMT) fold-changes are labeled in comparison with neutralization against XBB.1.5+F456L (the first line) and D614G (the second line). Two-tailed Wilcoxon signed-rank tests of paired samples are used. *, $p<0.05$; **, $p<0.01$; ***, $p<0.001$; ****, $p<0.0001$; NS, not significant ($p>0.05$).

(B) Logo plot for average escape scores on escape hotspots of Group A1/A2 antibodies in the DMS dataset. DMS were performed based on BA.5 RBD . Letters represent amino acids. Larger heights indicate stronger escape. Amino acids are colored according to chemical properties.

(C) IC50 of a panel of XBB.1.5-effetive monoclonal NAbs from Group A1 and A2 (determined by DMS) against XBB.1.5, XBB.1.5+L455F, XBB.1.5+F456L (EG.5), and XBB.1.5+L455F+F456L (XBB.1.5.70) pseudovirus. Dashed lines indicate limits of detection (10 μg/mL). Geometric mean IC50 values are labeled above the points. Two-tailed Wilcoxon signed-rank tests of paired samples are used. ***, $p<0.001$; ****, $p<0.0001$; NS, not significant ($p>0.05$).

(D) Neutralization of NAb drugs and selected monoclonal NAbs targeting NTD, RBD, or SD1 on the Spike glycoprotein against XBB.1.5, XBB.1.5+F456L (EG.5), and XBB.1.5+L455F+F456L (XBB.1.5.70) pseudovirus. Values shown in the grids are IC50 (μg/mL).

(E) ACE2-binding affinities of SARS-CoV-2 XBB subvariant RBD determined by SPR. Mean K_D values are annotated above the bars. Each point represents a replicate. Data from all replicates are shown. SPR assays are performed in at least two independent replicates.

METHODS DETAILS

Patient recruitment and plasma isolation

Blood samples from convalescent patients who had recovered from SARS-CoV-2 Omicron BTI or reinfection were obtained under the study protocols approved by Beijing Ditan Hospital, Capital Medical University (Ethics committee archiving No. LL-2021-024-02) and the Tianjin Municipal

Health Commission, and the Ethics Committee of Tianjin First Central Hospital (Ethics committee archiving No. 2022N045KY) (Table S1). Written informed consent, for the collection of information, storage and use of blood samples for research and data publication, was obtained from each participant.

The infections of patients in the BA.5 or BF.7 BTI cohort were confirmed between July and October 2022, during the "zero COVID" period in China. These infections were confirmed by PCR, and the viral strains of the majority of them were determined sequencing. Other samples which were not sequenced also showed strong epidemiological correlations with the sequenced samples.

Patients in the reinfection cohorts experienced first infections in December 2022 in Beijing and Tianjin. At that time, these regions were predominantly undergoing the BA.5/BF.7 wave[29]. Among the sequences from samples collected between 12/01/2022-02/01/2023, >98% of them were designated as BA.5* (excluding BQ*). Specifically, the major subtypes circulating in China at that time were BA.5.2.48* and BF.7.14*, which do not have additional mutations on RBD, and thus can be generally considered as BA.5/BF.7 (https://cov-spectrum.org/explore/China/AllSamples/from%3D2022-12-01%26to%3D2023-02-01/variants?&). Infections of patients in the XBB BTI and the second infections of patients in the reinfection cohorts were between May and June 2023, when >90% of uploaded sequences in Beijing were designated as XBB variants, and >85% were XBB* with S486P variants (https://cov-spectrum.org/explore/China/AllSamples/from%3D2023-05-01%26to%3D2023-06-15/variants?nextcladePangoLineage=XBB*&). These infections were confirmed via PCR test or antigen test.

Whole blood samples were diluted 1:1 with PBS+2% FBS and then subjected to Ficoll (Cytiva, 17-1440-03) gradient centrifugation. After centrifugation, plasma was collected from the upper layer. Plasma samples were aliquoted and stored at −20 °C or less and were heat-inactivated before experiments.

Pseudovirus neutralization assay

SARS-CoV-2 variants Spike pseudovirus was prepared based on a vesicular stomatitis virus (VSV) pseudovirus packaging system. Variants' spike plasmid is constructed into pcDNA3.1 vector. G*ΔG-VSV virus (VSV G pseudotyped virus, Kerafast) and spike protein plasmid were transfected to 293T cells (American Type Culture Collection [ATCC], CRL-3216). After culture, the

pseudovirus in the supernatant was harvested, filtered, aliquoted, and frozen at −80°C for further use.

Huh-7 cell line (Japanese Collection of Research Bioresources [JCRB], 0403) was used in pseudovirus neutralization assays. Plasma samples or antibodies were serially diluted in culture media and mixed with pseudovirus, and incubated for 1 h in a 37°C incubator with 5% CO_2. Digested Huh-7 cells were seeded in the antibody-virus mixture. After one day of culture in the incubator, the supernatant was discarded. D-luciferin reagent (PerkinElmer, 6066769) was added into the plates and incubated in darkness for 2 min, and cell lysis was transferred to the detection plates. The luminescence value was detected with a microplate spectrophotometer (PerkinElmer, HH3400). IC50 was determined by a four-parameter logistic regression model.

Antibody expression and purification

Antibody heavy and light chain genes were synthesized by GenScript, separately inserted into vector plasmids (pCMV3-CH, pCMV3-CL or pCMV3-CK) by infusion (Vazyme), and co-transfected into Expi293F cells (Thermo Fisher) using polyethylenimine transfection. The transfected cells were cultured at 36.5°C in 5% CO_2 and 175 rpm. for 6-10 days. The expression fluid was collected and centrifuged. After centrifugation, supernatants containing monoclonal antibodies were purified using Protein A magnetic beads (Genscript), and the purified samples were verified by SDS-PAGE.

Recombinant RBD expression and purification

DNA fragments that encode SARS-CoV-2 variant RBD (Spike 319-541) were codon-optimized for human cell expression and synthesized by Genscript. His-AVI tags were added at the end of the fragments. The fragments were then inserted into pCMV3 vector through infusion (Vazyme). The recombination products were transformed into E. coli DH5α competent cells (Tsingke). Colonies with the desired plasmids were confirmed by Sanger sequencing (Azenta) and cultured for plasmid extraction (CWBIO). 293F cells were transfected with the constructed plasmids and cultured for 6 days. Products were purified using Ni-NTA columns (Changzhou Smart-lifesciences, SA005100) and the purified samples were verified by SDS-PAGE.

Surface plasmon resonance

SPR experiments were performed on the Biacore 8K (Cytiva). Human ACE2 with Fc tag was immobilized onto Protein A sensor chips (Cytiva). Purified SARS-CoV-2 variant RBDs were prepared in serial dilutions (6.25, 12.5, 25, 50, and 100nM) and injected over the sensor chips. The

response units were recorded by Biacore 8K Evaluation Software 3.0 (Cytiva) at room temperature, and the raw data curves were fitted to a 1:1 binding model using Biacore 8K Evaluation Software 3.0 (Cytiva).

QUANTIFICATION AND STATISTICAL ANALYSIS

Surface plasmon resonance assays were performed in at least two independent replicates. SPR data were fitted to a 1:1 binding model using Biacore 8K Evaluation Software 3.0. Neutralization IC50 values were determined by a four-parameter logistic regression model. Wilcoxon signed-rank tests were used to determine the significance of differences in plasma NT50. Levels of significance were marked as: *, $p < 0.05$; **, $p < 0.01$; ***, $p < 0.001$; ****, $p < 0.0001$, as described in the corresponding figure legends.

Supplementary Tables and Figures

Table S1 | Information of SARS-CoV-2 patients involved in the study.

Figure S1 | SPR sensorgrams for the evaluation of RBD-hACE2 binding affinity

Related to Figure 2. SPR sensorgrams from experiments on hACE2-binding affinity of XBB.1.5, XBB.1.5+L455F, XBB.1.5+F456L, and XBB.1.5+L455F+F456L RBD. Representative results from at least two replicates are shown.

Figure S2 | L455F and F456L potentially affect interface conformation

Related to Figure 2.

(A) Interaction between XBB.1 RBD L455-F456 and ACE2 D30-K31 (PDB:8IOU).

(B) Mutagenesis that simulates L455F and L455F+F456L based on XBB.1 RBD-ACE2 complex structure (PDB:8IOU). F455 rotamers would clash with F456 (yellow box).

(C) Interaction between Omi-42 (Class 1 antibody) heavy chain and Beta RBD (PDB: 7ZR7).

References

1. Markov, P.V., Ghafari, M., Beer, M., Lythgoe, K., Simmonds, P., Stilianakis, N.I., and Katzourakis, A. (2023). The evolution of SARS-CoV-2. Nature Reviews Microbiology *21*, 361-379. 10.1038/s41579-023-00878-2.
2. Cao, Y., Yisimayi, A., Jian, F., Song, W., Xiao, T., Wang, L., Du, S., Wang, J., Li, Q., Chen, X.,

et al. (2022). BA.2.12.1, BA.4 and BA.5 escape antibodies elicited by Omicron infection. Nature *608*, 593-602. 10.1038/s41586-022-04980-y.

3. Jian, F., Yu, Y., Song, W., Yisimayi, A., Yu, L., Gao, Y., Zhang, N., Wang, Y., Shao, F., Hao, X., et al. (2022). Further humoral immunity evasion of emerging SARS-CoV-2 BA.4 and BA.5 subvariants. The Lancet Infectious Diseases *22*, 1535-1537. 10.1016/s1473-3099(22)00642-9.
4. Cao, Y., Song, W., Wang, L., Liu, P., Yue, C., Jian, F., Yu, Y., Yisimayi, A., Wang, P., Wang, Y., et al. (2022). Characterization of the enhanced infectivity and antibody evasion of Omicron BA.2.75. Cell Host Microbe. 10.1016/j.chom.2022.09.018.
5. Uraki, R., Ito, M., Kiso, M., Yamayoshi, S., Iwatsuki-Horimoto, K., Furusawa, Y., Sakai-Tagawa, Y., Imai, M., Koga, M., Yamamoto, S., et al. (2023). Antiviral and bivalent vaccine efficacy against an omicron XBB.1.5 isolate. The Lancet Infectious Diseases *23*, 402-403. 10.1016/S1473-3099(23)00070-1.
6. Yue, C., Song, W., Wang, L., Jian, F., Chen, X., Gao, F., Shen, Z., Wang, Y., Wang, X., and Cao, Y. (2023). ACE2 binding and antibody evasion in enhanced transmissibility of XBB.1.5. The Lancet Infectious Diseases *23*, 278-280. 10.1016/S1473-3099(23)00010-5.
7. Wang, Q., Iketani, S., Li, Z., Liu, L., Guo, Y., Huang, Y., Bowen, A.D., Liu, M., Wang, M., Yu, J., et al. (2023). Alarming antibody evasion properties of rising SARS-CoV-2 BQ and XBB subvariants. Cell *186*, 279-286 e278. 10.1016/j.cell.2022.12.018.
8. Kurhade, C., Zou, J., Xia, H., Liu, M., Chang, H.C., Ren, P., Xie, X., and Shi, P.Y. (2023). Low neutralization of SARS-CoV-2 Omicron BA.2.75.2, BQ.1.1 and XBB.1 by parental mRNA vaccine or a BA.5 bivalent booster. Nat Med *29*, 344-347. 10.1038/s41591-022-02162-x.
9. Cao, Y., Jian, F., Wang, J., Yu, Y., Song, W., Yisimayi, A., Wang, J., An, R., Chen, X., Zhang, N., et al. (2023). Imprinted SARS-CoV-2 humoral immunity induces convergent Omicron RBD evolution. Nature *614*, 521-529. 10.1038/s41586-022-05644-7.
10. Yamasoba, D., Uriu, K., Plianchaisuk, A., Kosugi, Y., Pan, L., Zahradnik, J., Ito, J., and Sato, K. (2023). Virological characteristics of the SARS-CoV-2 omicron XBB.1.16 variant. The Lancet Infectious Diseases *23*, 655-656. 10.1016/S1473-3099(23)00278-5.
11. Kaku, Y., Kosugi, Y., Uriu, K., Ito, J., Kuramochi, J., Sadamasu, K., Yoshimura, K., Asakura, H., Nagashima, M., Consortium, T.G.t.P.J., and Sato, K. (2023). Antiviral efficacy of the SARS-CoV-2 XBB breakthrough infection sera against Omicron subvariants including EG.5. bioRxiv, 2023.2008.2008.552415. 10.1101/2023.08.08.552415.
12. Dyer, O. (2023). Covid-19: Infections climb globally as EG.5 variant gains ground. BMJ *382*, p1900. 10.1136/bmj.p1900.
13. Chen, C., Nadeau, S., Yared, M., Voinov, P., Xie, N., Roemer, C., and Stadler, T. (2021). CoV-Spectrum: Analysis of Globally Shared SARS-CoV-2 Data to Identify and Characterize New Variants. Bioinformatics *38*, 1735-1737. 10.1093/bioinformatics/btab856.
14. Shu, Y., and McCauley, J. (2017). GISAID: Global initiative on sharing all influenza data – from vision to reality. Eurosurveillance *22*, 30494. doi:https://doi.org/10.2807/1560-7917.ES.2017.22.13.30494.
15. Cao, Y., Yisimayi, A., Bai, Y., Huang, W., Li, X., Zhang, Z., Yuan, T., An, R., Wang, J., Xiao, T., et al. (2021). Humoral immune response to circulating SARS-CoV-2 variants elicited by inactivated and RBD-subunit vaccines. Cell Res *31*, 732-741. 10.1038/s41422-021-00514-9.

16. Cao, Y., Hao, X., Wang, X., Wu, Q., Song, R., Zhao, D., Song, W., Wang, Y., Yisimayi, A., Wang, W., et al. (2022). Humoral immunogenicity and reactogenicity of CoronaVac or ZF2001 booster after two doses of inactivated vaccine. Cell Res *32*, 107-109. 10.1038/s41422-021-00596-5.
17. Park, Y.J., Pinto, D., Walls, A.C., Liu, Z., De Marco, A., Benigni, F., Zatta, F., Silacci-Fregni, C., Bassi, J., Sprouse, K.R., et al. (2022). Imprinted antibody responses against SARS-CoV-2 Omicron sublineages. Science *378*, 619-627. 10.1126/science.adc9127.
18. Yisimayi, A., Song, W., Wang, J., Jian, F., Yu, Y., Chen, X., Xu, Y., Yang, S., Niu, X., Xiao, T., et al. (2023). Repeated Omicron exposures override ancestral SARS-CoV-2 immune imprinting. bioRxiv, 2023.2005.2001.538516. 10.1101/2023.05.01.538516.
19. Nutalai, R., Zhou, D., Tuekprakhon, A., Ginn, H.M., Supasa, P., Liu, C., Huo, J., Mentzer, A.J., Duyvesteyn, H.M.E., Dijokaite-Guraliuc, A., et al. (2022). Potent cross-reactive antibodies following Omicron breakthrough in vaccinees. Cell *185*, 2116-2131 e2118. 10.1016/j.cell.2022.05.014.
20. Pinto, D., Park, Y.J., Beltramello, M., Walls, A.C., Tortorici, M.A., Bianchi, S., Jaconi, S., Culap, K., Zatta, F., De Marco, A., et al. (2020). Cross-neutralization of SARS-CoV-2 by a human monoclonal SARS-CoV antibody. Nature *583*, 290-295. 10.1038/s41586-020-2349-y.
21. Cao, Y., Jian, F., Zhang, Z., Yisimayi, A., Hao, X., Bao, L., Yuan, F., Yu, Y., Du, S., Wang, J., et al. (2022). Rational identification of potent and broad sarbecovirus-neutralizing antibody cocktails from SARS convalescents. Cell Rep *41*, 111845. 10.1016/j.celrep.2022.111845.
22. Hong, Q., Han, W., Li, J., Xu, S., Wang, Y., Xu, C., Li, Z., Wang, Y., Zhang, C., Huang, Z., and Cong, Y. (2022). Molecular basis of receptor binding and antibody neutralization of Omicron. Nature *604*, 546-552. 10.1038/s41586-022-04581-9.
23. Rochman, N.D., Faure, G., Wolf, Y.I., Freddolino, P.L., Zhang, F., and Koonin, E.V. (2022). Epistasis at the SARS-CoV-2 Receptor-Binding Domain Interface and the Propitiously Boring Implications for Vaccine Escape. mBio *13*, e00135-00122. doi:10.1128/mbio.00135-22.
24. Haddox, H.K., Galloway, J.G., Dadonaite, B., Bloom, J.D., IV, F.A.M., and DeWitt, W.S. (2023). Jointly modeling deep mutational scans identifies shifted mutational effects among SARS-CoV-2 spike homologs. bioRxiv, 2023.2007.2031.551037. 10.1101/2023.07.31.551037.
25. Starr, T.N., Greaney, A.J., Hannon, W.W., Loes, A.N., Hauser, K., Dillen, J.R., Ferri, E., Farrell, A.G., Dadonaite, B., McCallum, M., et al. (2022). Shifting mutational constraints in the SARS-CoV-2 receptor-binding domain during viral evolution. Science *377*, 420-424. 10.1126/science.abo7896.
26. Tamura, T., Ito, J., Uriu, K., Zahradnik, J., Kida, I., Anraku, Y., Nasser, H., Shofa, M., Oda, Y., Lytras, S., et al. (2023). Virological characteristics of the SARS-CoV-2 XBB variant derived from recombination of two Omicron subvariants. Nature Communications *14*, 2800. 10.1038/s41467-023-38435-3.
27. Park, Y.J., De Marco, A., Starr, T.N., Liu, Z., Pinto, D., Walls, A.C., Zatta, F., Zepeda, S.K., Bowen, J.E., Sprouse, K.R., et al. (2022). Antibody-mediated broad sarbecovirus neutralization through ACE2 molecular mimicry. Science *375*, 449-454. 10.1126/science.abm8143.
28. Ge, J., Wang, R., Ju, B., Zhang, Q., Sun, J., Chen, P., Zhang, S., Tian, Y., Shan, S., Cheng, L., et al. (2021). Antibody neutralization of SARS-CoV-2 through ACE2 receptor mimicry. Nat

Commun *12*, 250. 10.1038/s41467-020-20501-9.

29. Pan, Y., Wang, L., Feng, Z., Xu, H., Li, F., Shen, Y., Zhang, D., Liu, W.J., Gao, G.F., and Wang, Q. (2023). Characterisation of SARS-CoV-2 variants in Beijing during 2022: an epidemiological and phylogenetic analysis. Lancet *401*, 664-672. 10.1016/S0140-6736(23)00129-0.

Figure 1

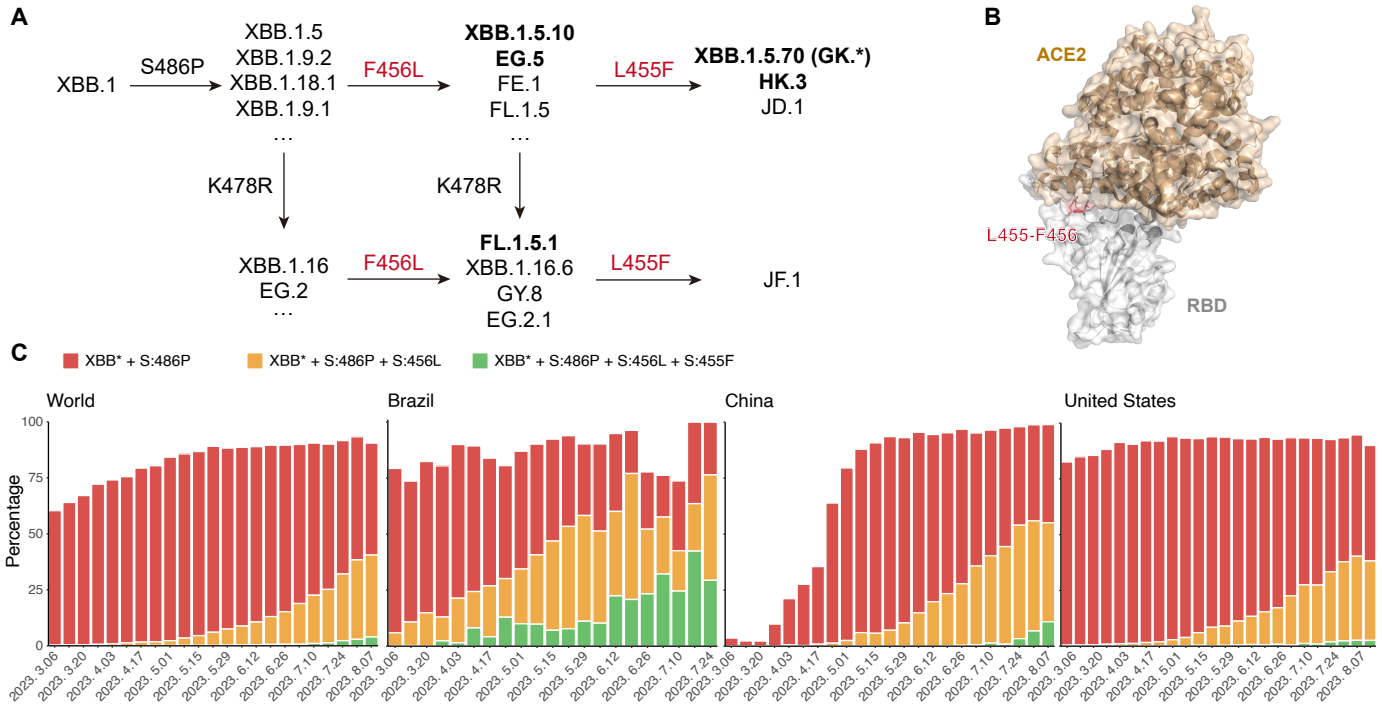
A
XBB.1
S486P
XBB.1.5
XBB.1.9.2
XBB.1.18.1
XBB.1.9.1
…
F456L
XBB.1.5.10
EG.5
FE.1
FL.1.5
…
L455F
XBB.1.5.70 (GK.*)
HK.3
JD.1
K478R
XBB.1.16
EG.2
…
F456L
FL.1.5.1
XBB.1.16.6
GY.8
EG.2.1
L455F
JF.1
B
ACE2
L455-F456
RBD
C
XBB* + S:486P
XBB* + S:486P + S:456L
XBB* + S:486P + S:456L + S:455F
World
Brazil
China
United States
Percentage
100
75
50
25
0
2023.3.06
2023.3.20
2023.4.03
2023.4.17
2023.5.01
2023.5.15
2023.5.29
2023.6.12
2023.6.26
2023.7.10
2023.7.24
2023.8.07

Figure 2

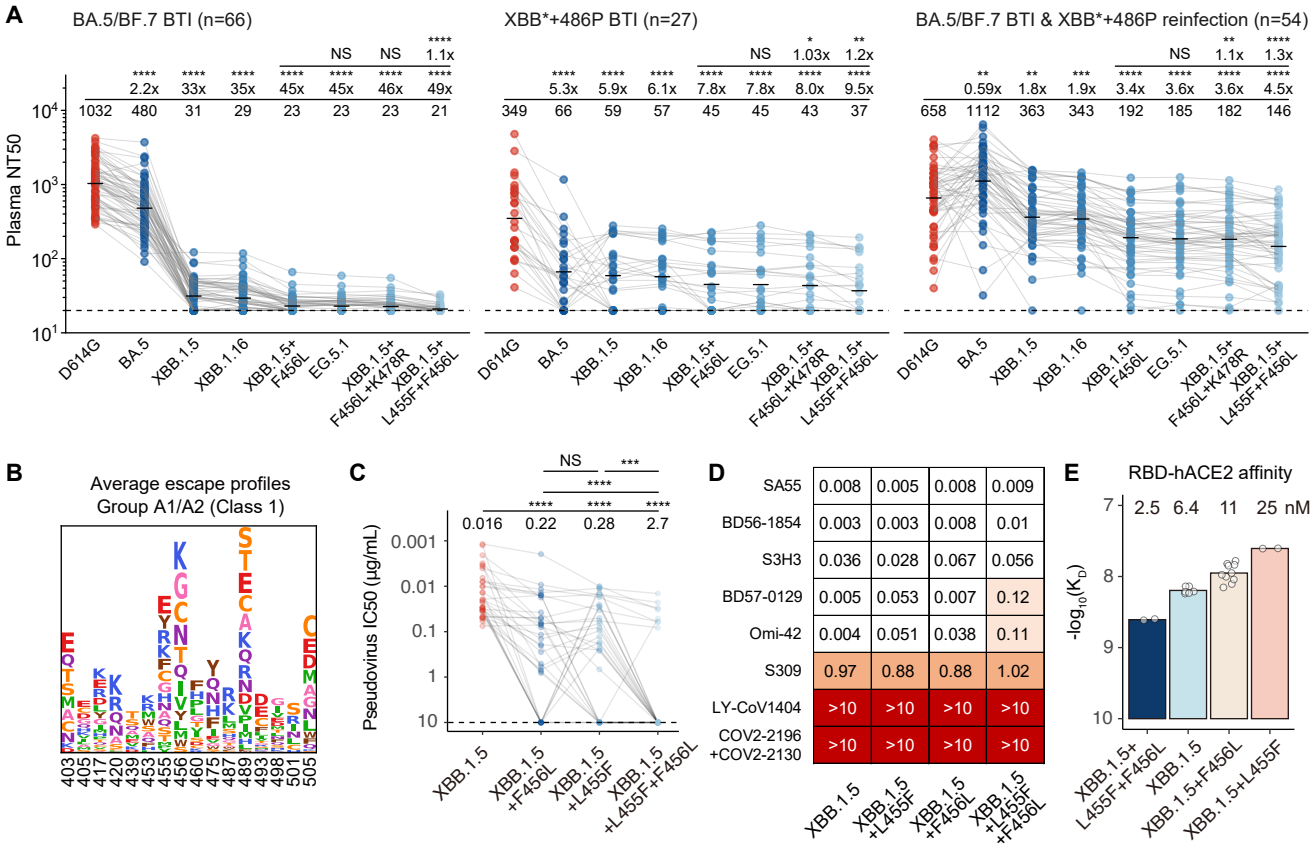
A
BA.5/BF.7 BTI (n=66)
XBB*+486P BTI (n=27)
BA.5/BF.7 BTI & XBB*+486P reinfection (n=54)
Plasma NT50
D614G
BA.5
XBB.1.5
XBB.1.16
XBB.1.5+ F456L
EG.5.1
XBB.1.5+ F456L+K478R
XBB.1.5+ L455F+F456L
B
Average escape profiles
Group A1/A2 (Class 1)
C
Pseudovirus IC50 (μg/mL)
0.016
0.22
0.28
2.7
XBB.1.5
XBB.1.5 +F456L
XBB.1.5 +L455F
XBB.1.5 +L455F+F456L
D
SA55
BD56-1854
S3H3
BD57-0129
Omi-42
S309
LY-CoV1404
COV2-2196 +COV2-2130
E
RBD-hACE2 affinity
2.5 6.4 11 25 nM
-log10(KD)
XBB.1.5+ L455F+F456L
XBB.1.5
XBB.1.5+F456L
XBB.1.5+L455F

Figure S1

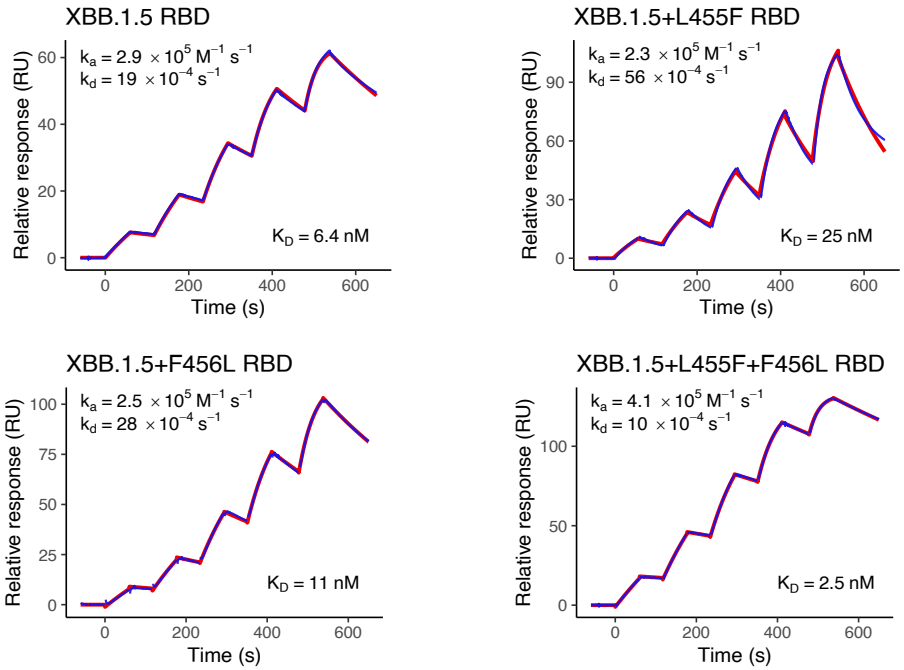
XBB.1.5 RBD
$k_a = 2.9 \times 10^5\ M^{-1}\ s^{-1}$
$k_d = 19 \times 10^{-4}\ s^{-1}$
$K_D = 6.4$ nM
XBB.1.5+L455F RBD
$k_a = 2.3 \times 10^5\ M^{-1}\ s^{-1}$
$k_d = 56 \times 10^{-4}\ s^{-1}$
$K_D = 25$ nM
XBB.1.5+F456L RBD
$k_a = 2.5 \times 10^5\ M^{-1}\ s^{-1}$
$k_d = 28 \times 10^{-4}\ s^{-1}$
$K_D = 11$ nM
XBB.1.5+L455F+F456L RBD
$k_a = 4.1 \times 10^5\ M^{-1}\ s^{-1}$
$k_d = 10 \times 10^{-4}\ s^{-1}$
$K_D = 2.5$ nM
Relative response (RU)
Time (s)

Figure S2

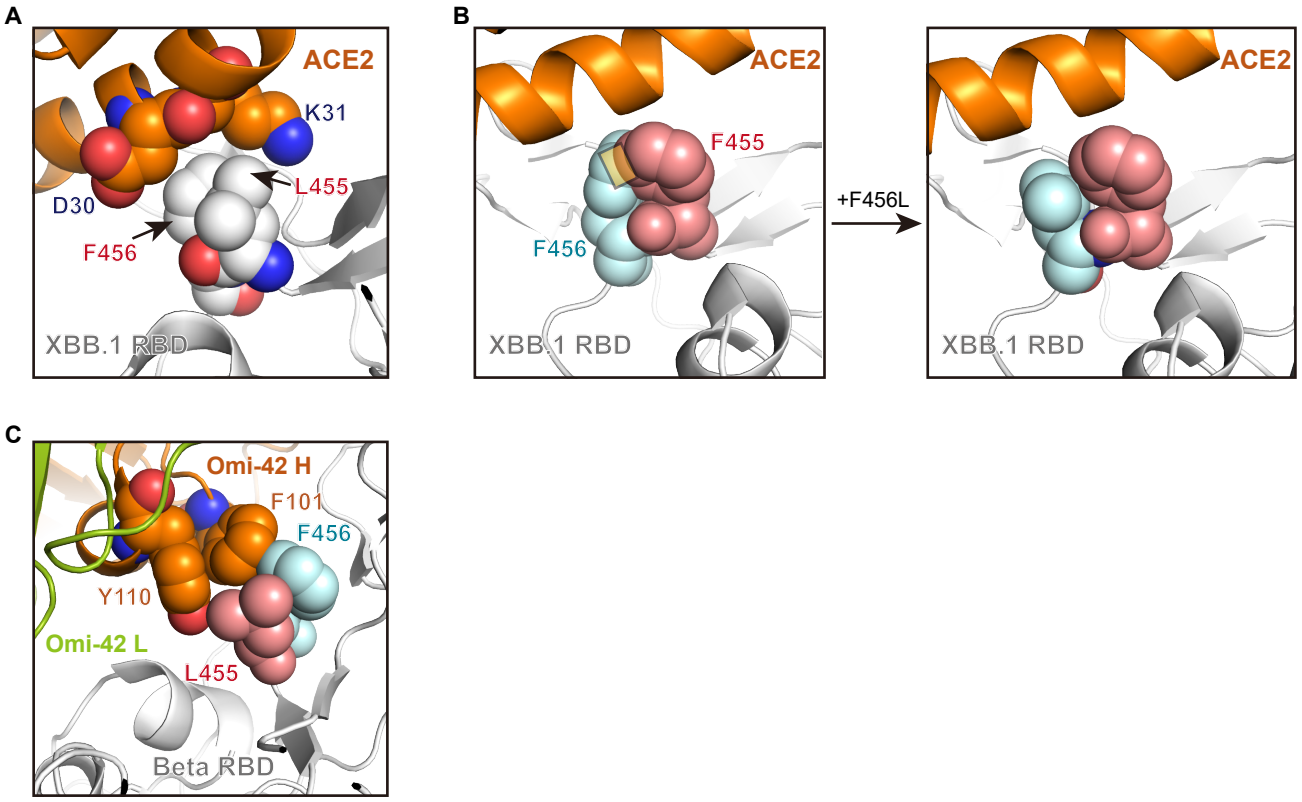
A
ACE2
K31
L455
D30
F456
XBB.1 RBD
B
ACE2
F455
F456
XBB.1 RBD
+F456L
ACE2
XBB.1 RBD
C
Omi-42 H
F101
F456
Y110
Omi-42 L
L455
Beta RBD